doi:10.1093/brain/awy172 BRAIN 2018: 141; 2289–2298 | 2289

BRAIN
A JOURNAL OF NEUROLOGY

A novel complex neurological phenotype due to a homozygous mutation in *FDX2*

Juliana Gurgel-Giannetti,[1]* David S. Lynch,[2,3]* Anderson Rodrigues Brandão de Paiva,[4] Leandro Tavares Lucato,[5] Guilherme Yamamoto,[6] Christer Thomsen,[7] Somsuvro Basu,[8] Fernando Freua,[4] Alexandre Varella Giannetti,[9] Bruno Della Ripa de Assis,[4] Mara Dell Ospedale Ribeiro,[4] Isabella Barcelos,[4] Katiane Sayão Souza,[4] Fernanda Monti,[4] Uirá Souto Melo,[6] Simone Amorim,[4] Leonardo G. L. Silva,[6] Lúcia Inês Macedo-Souza,[6] Angela M. Vianna-Morgante,[6] Michio Hirano,[10] Marjo S. Van der Knaap,[11] Roland Lill,[8,12] Mariz Vainzof,[6] Anders Oldfors,[7] Henry Houlden[2,3] and Fernando Kok[4,6]

*These authors contributed equally to this work.

Defects in iron–sulphur [Fe-S] cluster biogenesis are increasingly recognized as causing neurological disease. Mutations in a number of genes that encode proteins involved in mitochondrial [Fe-S] protein assembly lead to complex neurological phenotypes. One class of proteins essential in the early cluster assembly are ferredoxins. FDX2 is ubiquitously expressed and is essential in the *de novo* formation of [2Fe-2S] clusters in humans. We describe and genetically define a novel complex neurological syndrome identified in two Brazilian families, with a novel homozygous mutation in *FDX2*. Patients were clinically evaluated, underwent MRI, nerve conduction studies, EMG and muscle biopsy. To define the genetic aetiology, a combination of homozygosity mapping and whole exome sequencing was performed. We identified six patients from two apparently unrelated families with autosomal recessive inheritance of a complex neurological phenotype involving optic atrophy and nystagmus developing by age 3, followed by myopathy and recurrent episodes of cramps, myalgia and muscle weakness in the first or second decade of life. Sensory-motor axonal neuropathy led to progressive distal weakness. MRI disclosed a reversible or partially reversible leukoencephalopathy. Muscle biopsy demonstrated an unusual pattern of regional succinate dehydrogenase and cytochrome *c* oxidase deficiency with iron accumulation. The phenotype was mapped in both families to the same homozygous missense mutation in *FDX2* (c.431C > T, p.P144L). The deleterious effect of the mutation was validated by real-time reverse transcription polymerase chain reaction and western blot analysis, which demonstrated normal expression of *FDX2* mRNA but severely reduced expression of FDX2 protein in muscle tissue. This study describes a novel complex neurological phenotype with unusual MRI and muscle biopsy features, conclusively mapped to a mutation in *FDX2*, which encodes a ubiquitously expressed mitochondrial ferredoxin essential for early [Fe-S] cluster biogenesis.

1 Department of Paediatrics, Universidade Federal de Minas Gerais, Belo Horizonte, Brazil
2 Department of Molecular Neuroscience, UCL Institute of Neurology, London, UK
3 Leonard Wolfson Experimental Neurology Centre, UCL Institute of Neurology, London, UK
4 Neurogenetics Unit, Neurology Department, Hospital das Clínicas da Universidade de São Paulo, São Paulo, Brazil
5 Neuroradiology Section, Hospital das Clínicas da Universidade de São Paulo, São Paulo, Brazil
6 Human Genome and Stem Cell Research Center, Department of Genetics and Evolutionary Biology, Instituto de Biociências, Universidade de São Paulo, São Paulo, Brazil
7 Department of Pathology and Genetics, Sahlgrenska University Hospital, University of Gothenburg, Sweden
8 Institute for Cytobiology and Cytopathology, Philipps-Universität Marburg, Robert-Koch-Strasse 6, 35032 Marburg, Germany
9 Department of Surgery, Federal University of Minas Gerais, Belo Horizonte, Brazil

Received November 15, 2017. Revised March 30, 2018. Accepted April 26, 2018. Advance Access publication July 13, 2018

10 Department of Neurology, Columbia University Medical Center, New York, USA
11 Department of Child Neurology, VU University Medical Center, Amsterdam, The Netherlands
12 LOEWE Center for Synthetic Microbiology, SynMikro, Hans-Meerwein-Strasse, 35043 Marburg, Germany

Correspondence to: Dr Juliana Gurgel Giannetti
Rua Santa Catarina 1042, 201, Belo Horizonte, Brazil
E-mail: gurgelju@yahoo.com.br

Correspondence may also be addressed to: Dr David Lynch
Department of Molecular Neuroscience, UCL Institute of Neurology, Queen Square, London, WC1N 3BG UK
E-mail: david.lynch.13@ucl.ac.uk

Keywords: FDX2; brain; nerve; muscle; optic atrophy

Abbreviations: [Fe-S] = iron–sulphur; COX = cytochrome *c* oxidase; SDH = succinate dehydrogenase

Introduction

Iron–sulphur [Fe-S] clusters are essential biological cofactors found in all living organisms, from archaea to eukaryotes (Fontecave, 2006; Lill, 2009). They consist of protein-bound Fe ions, linked by sulphide bridges and are essential in a large number of electron transfer reactions. [Fe-S] clusters are almost unique in their ability to access various redox states over a wide range, with electron transport roles in critical processes like the mitochondrial respiratory chain. [Fe-S] clusters have also been found to play important roles in more diverse cellular pathways from catalysis to gene regulation (Beinert *et al.*, 1997; Rouault, 2015). The biogenesis of [Fe/S] proteins in the mitochondria is a complex process and takes place in several stages (Braymer and Lill, 2017). The early stage of biogenesis involves a cysteine desulphurase as a source of sulphur and frataxin as a potential source of iron, with the cluster being formed on the scaffold protein iron-sulphur cluster assembly enzyme (ISCU). The newly made [2Fe-2S] cluster is then transferred to numerous downstream biogenesis proteins that will use the cofactor for transfer to target [Fe/S] proteins such as the subunits of mitochondrial complexes I and II.

Another class of proteins essential for *de novo* [2Fe-2S] cluster assembly on ISCU are ferredoxins (Webert *et al.*, 2014; Boniecki *et al.*, 2017). Humans possess two ferredoxins, *FDX1* and *FDX2* (formerly FDX1L) (Sheftel *et al.*, 2010). While both proteins localize to the mitochondrion, expression of *FDX1* is highest in the adrenal gland, where the protein functions in the steroid synthesis pathway. *FDX2*, however, is ubiquitously expressed and is essential in the formation of [Fe-S] clusters in humans (Sheftel *et al.*, 2010).

Mutations in a number of genes that encode proteins involved in [Fe-S] cluster assembly lead to complex neurological phenotypes (Stehling *et al.*, 2014). The most common of these syndromes is Friedreich's ataxia, an autosomal recessive multisystem neurodegenerative disorder characterized by ataxia, peripheral neuropathy and cardiomyopathy (Beilschmidt and Puccio, 2014). It is typically caused by a trinucleotide repeat intronic expansion in *FXN*, encoding frataxin (Dürr *et al.*, 1996). Loss of function mutations in *ISCU* lead to myopathy with severe exercise intolerance (Mochel *et al.*, 2008; Olsson *et al.*, 2008; Nordin *et al.*, 2011; Legati *et al.*, 2017) and mutations in *NUBPL*, an [Fe-S] protein involved in complex I assembly (Sheftel *et al.*, 2009), lead to leukoencephalopathy, ataxia and developmental regression (Calvo *et al.*, 2010). In 2014, a single case was described with isolated mitochondrial myopathy due to a homozygous translation start site mutation in *FDX2* (Spiegel *et al.*, 2014). More recently, mutations in *FDXR*, encoding ferredoxin reductase, were described in eight patients with a syndrome including hearing loss, optic atrophy and sensory neuropathy (Paul *et al.*, 2017).

In this study, we describe the clinical phenotype of six patients from two apparently unrelated Brazilian families but living in the same geographic region with a complex phenotype including optic atrophy, reversible leukoencephalopathy, mitochondrial myopathy with exercise intolerance and axonal polyneuropathy and, in some patients, pyramidal signs. Using a combination of homozygosity mapping and whole exome sequencing, we mapped this phenotype to the same homozygous, deleterious mutation in *FDX2*.

Materials and methods

Subjects

Clinical evaluation was performed on both families by two independent research groups that shared their data. All patients were clinically and neurologically evaluated, and underwent EMG and nerve conduction studies and muscle biopsy.

We received approval of the ethical standards committee at both institutions (São Paulo University and Federal University of Minas Gerais) and written informed consent was obtained from all included family members.

Neuroimaging

All patients underwent at least one exam. We analysed 13 brain MRIs performed at different ages ranging from 8

months to 41 years. Since MRIs were performed in different centres, analysis was based mainly on multiplanar FLAIR, T_1 and T_2-weighted images. Intensity of T_2 changes were graded in a semi-quantitative manner as absent, mild, moderate or severe. Diffusion-weighted images and apparent diffusion coefficient maps, when available, were scrutinized in the search for lesions with restricted diffusion. Magnetic resonance spectroscopy was also analysed when available, and we focused on the detection of lactate peaks.

Muscle biopsy

Muscle biopsies were performed on the biceps brachialis and cryostat sections were obtained with 8 µm thickness. Conventional histochemical techniques were performed: haematoxylin and eosin, modified Gomori trichrome, Periodic acid–Schiff technique, Oil Red O, reduced nicotinamide adenine dinucleotide dehydrogenase-tetrazolium reductase (NADH-TR), succinate dehydrogenase (SDH), cytochrome *c* oxidase (COX), and adenosine triphosphatase (ATPase) preincubated at pH 9.4, 4.63 and 4.35. Perls' Prussian Blue staining was performed as described (Stevens, 1990) and with DAB enhancement (Mochel, 2008) to identify iron deposition.

For immunohistochemistry, 8 µm sections were fixed in 4% formaldehyde at 4°C for 10 min, washed in Tris-buffered saline-Tween 20 (TBS-T) for 10 min, permeabilized in a graded methanol series (70% 10 min, 95% 10 min, 100% 20 min, 95% 10 min, 70% 10 min), washed in TBS-T for 5 min and further processed in a Dako Autostainer using the Dako EnVision™ FLEX High pH kit. The following antibodies were applied for 1 h: anti-SDHB ab14714 Abcam (1:500), anti-MTCO1 ab14705 Abcam (1:2000) and anti-VDAC1 ab14734 Abcam (1:2000).

Electron microscopy was performed on tissue specimens that had been fixed in glutaraldehyde, post-fixed in OsO_4 and embedded in resin. Ultrathin sections were contrasted with uranyl acetate and lead citrate.

The respiratory chain enzyme analysis was performed on frozen tissue using spectrophotometry (DiMauro *et al.*, 1987).

Molecular analysis

Genome wide genotyping was performed on Patients 1–4, both parents and an unaffected sibling from Family 1 using the Axiom® Genome-Wide LAT 1 Array (Affymetrix). Runs of homozygosity were identified using PLINK software (Purcell *et al.*, 2007). Whole exome sequencing was performed on Patients 3 and 4 from Family 1 and in four members (Patients 5, 6 and parents of Patient 5) from Family 2 using the Agilent SureSelect Exon Enrichment kit. Segregation of the *FDX2* mutation was confirmed by Sanger sequencing of *FDX2* exon 5 using the following primer sequences: Forward: 5′-ATCCTCCCCACTTCCAGTTC-3′; Reverse: 5′-TCTTAAGC TCCTGGCCTCAA-3′.

Prior to whole exome sequencing, Sanger sequencing of *EARS2*, *SDHA* and *SDHB* was performed in Patient 5, and no potential pathogenic variant was identified in homozygosity or compound heterozygosity in this subject. Cytogenetic investigation was performed on cultured peripheral blood lymphocytes from Patient 1 and her parents, including G- and C-banding, and fluorescent *in situ* hybridization (FISH) analyses.

Functional studies

Human RNA extraction, cDNA synthesis and RT-qPCR

RNA extracted from muscle from four patients and two healthy controls was used for quantitative reverse transcription PCR (RT-qPCR). RNA extraction was performed using TRIzol® (ThermoFisher Scientific) and RNA quality was evaluated by agarose gel electrophoresis; and all samples had 260:230 ratio above 1.90, measured using a NanoDrop (ThermoFisher Scientific). Total RNA (1 µg/µl) was reverse-transcribed with oligo(dT) primers using SuperScript™ III First-strand Synthesis System (ThermoFisher Scientific). *FDX2* primers for RT-qPCR spanned the exon 4–5 junction: Forward 5′- GTGAGTGAAGACCACCTGGAT-3′; Reverse 5′- GCCA TGTCTAGCATGTCGTC-3′.

RT-qPCR was normalized to *TBP* and the cDNA amplification was performed using Applied Biosystems® 7500 Fast Real-time PCR System. Relative gene expression was calculated using $2^{-\Delta\Delta CT}$ method (Schmittgen and Livak, 2008). Each experiment was performed in triplicate considering standard deviation of triplicate positive when <0.1.

Western blot study

Muscle tissue was lysed in RIPA buffer (Pierce) and protein concentration was determined with Pierce 660 nm protein assay. Lysed skeletal muscle samples were subjected to SDS-PAGE (6–18% gradient gel; Stehling *et al.*, 2018) and immunostaining. Antibodies were targeted against FDX2 (affinity purified, Sheftel *et al.*, 2010), F1 α/β subunits of complex V (kind gift of Drs H. Schägger and I. Wittig, 1:1000), VDAC (Cell Signalling Technology, 1:1000), tubulin (Sigma, 1:10 000), and actin (BD Transduction Laboratories, 1:2000).

Results

We identified six patients from two apparently unrelated Brazilian families living in the same geographic area with a complex multisystem phenotype: childhood onset of optic atrophy, recurrent episodes of myalgia and/or proximal weakness, axonal polyneuropathy, pyramidal signs (present in two patients) and reversible or partially reversible leukoencephalopathy on MRI. A summary of clinical findings is presented in Tables 1 and 2, and a simplified pedigree of Families 1 and 2 is shown in Fig. 1.

Clinical findings

The first recognizable clinical sign in all patients was nystagmus, secondary to low visual acuity caused by non-progressive optic atrophy, seen before the age of 3 years in all patients. A mild motor delay was observed in all patients, except Patient 1, who had a global developmental delay, and Patient 5, who had a normal development.

In all patients there was evidence of recurrent episodes of cramps, myalgia and muscle weakness, often precipitated

Table 1 Summary of clinical findings

Patient	Current age	Age of onset	First symptoms	Developmental delay	Nystagmus/ optic atrophy	Exercise-induced myalgia/ myopathy	Axonal sensori-motor polyneuropathy	Endocrine abnormalities		Haematological abnormalities	
								Subclinical hypothyroidism	Type II diabetes	Neutropaenia	Microcytic anaemia
P1	13 y	<6 m	Floppy baby	Global	+	+ (eo)	+	+	–	+	+
P2	6 y	1 y 4 m	Nystagmus, LVA	Minor motor[a]	+	+ (eo)	–	+	–	+	+
P3	29 y	1 y	Nystagmus, LVA	Minor motor[a]	+	+ (to)	+	+	–	+	+
P4	34 y	1 y	Nystagmus, LVA	Minor motor[a]	+	+ (to)	+	NA	+ (ao)	+	+
P5	11 y	8 m	Nystagmus, LVA	–	+	+ (eo)	–	–	–	–	–
P6	41 y	6 m	Nystagmus, LVA	Minor motor[a]	+	+ (eo)	+	–	+ (+ + + ao)	–	–

[a]Patients walked at around 2 years of age. + = present; – = absent; ao = adult-onset; eo = early-onset; LVA = low visual acuity; NA = not available; to = teenage-onset.

by exercise, infections or low temperature. These events started in childhood or adolescence, sometimes leading to temporary loss of ambulation for 1 to 3 weeks. In Patient 5, a creatine kinase level during an episode was >3000 U/l, indicating rhabdomyolysis.

Motor features included a combination of myopathy, upper motor neuron dysfunction and sensori-motor axonal neuropathy. Weakness was progressive in Patient 6, who became wheelchair-bound at the age of 33 years. Hypoactive deep tendon reflexes were seen in all individuals, except Patient 5. Babinski signs with mild spasticity were seen in Patients 3 and 4. Sensory ataxia, characterized by positive Romberg sign and decreased vibration and position sensitivity, was present in Patients 3 and 4. Permanent weakness was related to age and disease duration, since it was present in two of the three adult patients: Patient 3 had proximal and distal involvement, and Patient 6 only distal weakness. Clinical features of neuropathy and abnormal nerve conduction study were seen in all four older patients with more than 10 years of age. Finally, ptosis was seen in Patients 3 and 6 (Table 2).

In Family 1, all tested members (Patients 1–4) had mild microcytic anaemia without iron deficiency, sometimes accompanied by thrombocytopaenia or neutropaenia.

All patients underwent nerve conduction studies and EMG, which showed sensori-motor polyneuropathy in Patients 1, 3, 4 and 6, but no abnormalities in Patients 2 and 5.

Additionally, Patient 1 had global developmental delay, intellectual disability and dysmorphic features, characterized by protruding ears, micrognathia, high arched palate, almond-shaped eyes, high nasal bridge, dolicocephaly, and brachydactyly. The dysmorphic features were thought to be due to an unrelated and separate condition not affecting the other five patients described here.

Neuroimaging

The common finding observed in brain MRI from all patients was the presence of hypoplastic optic nerves and chiasm (Fig. 2). In three patients, magnetic resonance abnormalities progressed in a somewhat similar fashion (Patients 1, 2 and 5). In Patient 2 the first exam done at 1 year and 8 months demonstrated T_2 hyperintensity involving subcortical and deep cerebral white matter and corpus callosum (genu and splenium), associated with restricted diffusion. There was also mild pontine T_2 hyperintensity sparing both corticospinal tracts and some thinning of the isthmus of the corpus callosum. Magnetic resonance findings were more evident between 3 and 5 years of age, not only the white matter lesions, but also the pontine changes and a peculiar pattern of thalamic involvement. This pattern was characterized by T_2 hyperintensity and restricted diffusion in anterior nuclei, sparing mammillothalamic tracts and extending also to the internal medullary lamina.

By the age of 7 to 9 years of life, MRI changes presented remarkable improvement. In two patients, Patients 1 and 5, MRI exams at this age became essentially normal, except

Table 2 Summary of the neurological findings

Patient	Learning disability	Low visual acuity and optic atrophy	Ptosis	Proximal weakness	Distal weakness	Pes cavus	Sensory abnormalities	DTRs	Spasticity	Babinski sign
P1	+	+	+	–	–	+	–	H	–	–
P2	–	+	–	–	–	–	–	H	–	–
P3	–	+	+	+	+	+	+	H	Mild	+
P4	–	+	–	–	–	+	+	H	Mild	+
P5	–	+	–	–	–	–	–	N	–	–
P6	–	+	+	–	+	+	+	H	–	–

+ = present; – = absent; DTRs = deep tendon reflexes; H = hypoactive; N = normoactive.

Table 3 Summary of the neuroimaging findings from the six patients performed at different ages

Age	Case/MR number	Subcortical white matter (T_2 hypertensity)	Thalamus (T_2 hypertensity)	Brainstem (T_2 hypertensity)	DWI hyperintensity	Restricted diffusion (ADC map)	Corpus callosum (thinning)	MRS (lactate peaks)
8 m	P1/01	+	–	–	NA	NA	Mild global; posterior predominance	NA
1 y 8 m	P2/01	+ +	+	+	Yes	Yes	Isthmus	NA
3 y	P2/02	+ + +	+ + +	+ + +	Yes	No (facilitated diffusion)	Isthmus	NA
3 y	P5/01	+ + +	+ + +	+ + +	Yes	NA	Isthmus	Yes
5 y	P1/02	+ + +	+ +	+ +	Yes	NA	Mild global; posterior predominance	NA
6 y	P5/02	+ +	+	+	Yes	Yes	Isthmus	Yes
7 y	P5/03	+	+	+	Yes	Yes	Isthmus	NA
9 y	P5/04	–	–	–	No	No	Isthmus	No
9 y	P1/03	+	–	+	Yes	Yes	Mild global; posterior predominance	No
10 y	P1/04	–	–	+	No	No	Mild global; posterior predominance	No
Adult	P3/01	+	–	–	No	No	Mild global; posterior predominance	No
Adult	P4/01	–	–	–	No	No	Normal	NA
Adult	P6/01	–	–	–	No	No	Normal	No

ADC = apparent diffusion coefficient; DWI = diffusion-weighted image; MR = magnetic resonance; NA = not available. T_2-hyperintensity changes were graded using a semiquantitative scale: absent (–); mild (+); moderate (+ +) and severe (+ + +).

for some callosal thinning. In two patients (Patients 4 and 6), brain imaging was obtained at adult life and the exams were otherwise normal (except for the optic pathway involvement). In the youngest adult patient (Patient 3) there were also patchy T_2 hyperintense abnormalities throughout the supratentorial white matter (without diffusion changes) and reduced thickness of the corpus callosum, particularly the posterior portions.

Lactate peaks were found using magnetic resonance spectroscopy in only one patient (Patient 5), from the four patients who had at least one magnetic resonance spectroscopy exam in our series. In this patient lactate peaks were found when the patient presented significant structural MRI changes (at 3 and 6 years old), and were not present when structural MRI was essentially normal (at age 9). In the other three patients the magnetic resonance spectroscopy was performed when the brain MRI has mild white matter abnormalities (Patients 1 and 3) or when it was normal (Patient 5).

In Patients 1, 2 and 5, who were clinically evaluated at the time that the brain magnetic resonance showed the white matter, thalamus and brainstem abnormalities, there was no evidence of any pyramidal or extrapyramidal signs in the neurological examination. Only one patient was submitted to an MRI during the first year of life, at the age of 8 months, and this exam revealed some widening of the lateral ventricles and mild diffuse T_2 hyperintensity in white matter (suggesting at least some delay in myelination) (Patient 1). However, this patient has also a coincidental chromosomal abnormality.

Muscle pathology

Patients 3–6 underwent muscle biopsy and in all samples there was the presence of ragged red fibres and SDH and COX negative fibres. Respiratory chain enzyme analysis was only performed in Patient 5 and showed no abnormalities. In Patient 5, the muscle biopsy was performed at 3

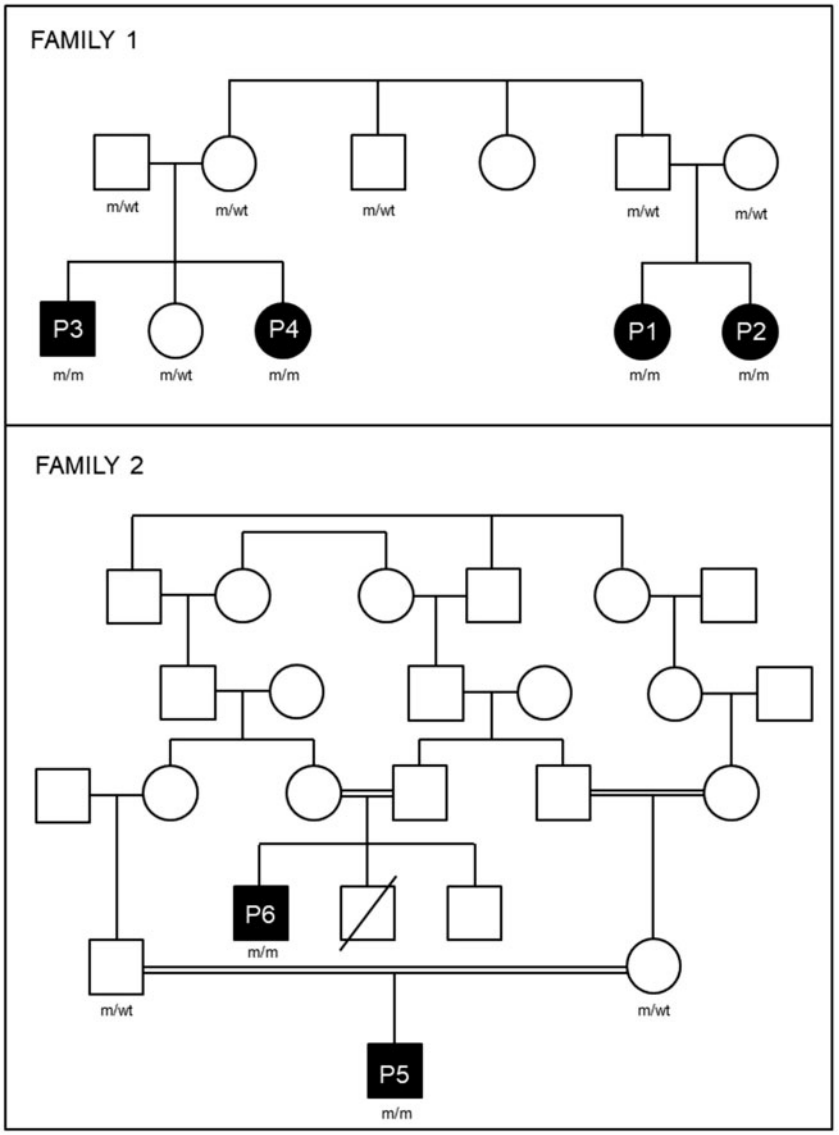

Figure 1 Pedigree of Families 1 and 2. Filled boxes are affected members and unfilled boxes are unaffected. Genotypes are shown where m = mutant, wt = wild type.

years of age and the proportion of ragged red fibres was less frequent than in the others patients. The other three patients (Patients 3, 4 and 6) underwent muscle biopsy in adult life.

In Patient 3, the muscle showed more intense alterations, which are illustrated in Fig. 3.

There were SDH- and COX-negative fibres that were clustered together in patch-like areas (Fig. 3A and B). Furthermore, punctate iron accumulation was observed in SDH and COX deficient fibres by iron staining (Fig. 3C). Electron microscopy revealed mitochondrial paracrystalline inclusions in numerous fibres. In these fibres frequent electron-dense irregular inclusions were identified that presumably represent iron deposition in the mitochondria (Fig. 3D). Immunohistochemical analysis of complex II and complex IV subunits showed markedly reduced expression in fibres with low SDH and COX enzymatic activity (Fig. 3E, F, H and I) while mitochondrial mass was increased as revealed by the mitochondrial marker VDAC1 (porin; Fig. 3G).

Genetic results

Genome-wide homozygosity mapping in all affected members of Family 1 revealed two shared homozygous regions, a 1 Mb region on Chromosome 19 (Chr19: 9400194–10492040) and a 500 kb region on Chromosome 2 (Chr2: 89469319–89994709). We next examined the whole exome sequencing data from Family 1, limiting our analysis to rare, homozygous variants that were not synonymous or intronic and mapped within the regions of homozygosity identified. The only such variant detected

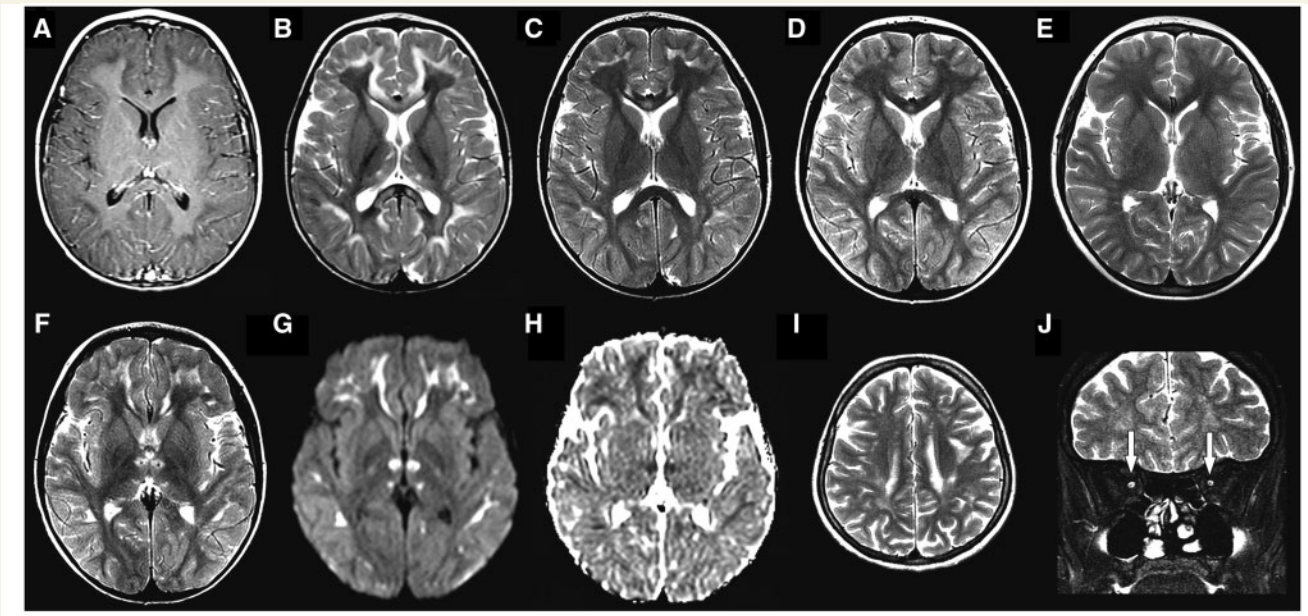

Figure 2 Neuroimaging findings. In Subject 5, at age 3 years, axial T_1-weighted post-contrast image (**A**) demonstrates hypointensity in the subcortical white matter, without abnormal enhancement. Axial T_2-weighted images from the same patient at ages 3 (**B**), 6 (**C**), 7 (**D**) and 9 years (**E**) disclose progressive improvement of T_2 hyperintense abnormalities in thalami, subcortical white matter and corpus callosum, initially appreciated in **B**. Axial T_2-weighted image from the same patient at age 6 years (**F**) shows sparing of mammillothalamic tracts, seen as T_2 hypointense dots in the centre of the signal change in the anterior portion of thalami. Considering the subsequent improvement, the restricted diffusion [hyperintensity in diffusion image (**G**) and hypointensity in apparent diffusion coefficients map (**H**)] probably reflects intramyelinic oedema. Axial and coronal T_2-weighted images from Subject 3 at age 27 years (**I** and **J**), demonstrate residual T_2 hyperintensity in subcortical white matter (**I**) and hypoplasia of both optic nerves (arrows in **J**).

was in *FDX2* (NM_001031734 c.431C > T, p.P144L). This variant was not found in the ExAC or 1000G databases but was found in the heterozygous state in 1 of 600 controls from the Brazilian ABraOM database (minor allele frequency: 0.000821) (Naslavsky *et al.*, 2017). We validated the variant by Sanger sequencing, confirming that all affected family members were homozygous, whereas the patients' parents and an unaffected sibling were all heterozygous. Patient 1, who had some additional dysmorphic features not seen in the other five patients described, was found to carry a coincidental tetrasomy for the short arm of chromosome 9, karyotype: 46,XX, + i(9)(p10). Both her parents had normal karyotypes.

Family 2 underwent independent genetic studies. The index case (Patient 5) was first investigated for mutations in *EARS2* (Steeweg *et al.*, 2012), because of the reversible leukoencephalopathy, and for mutations in the *SDHA* and *SDHB* (Alston *et al.*, 2012), based on the presence of SDH negative fibres in muscle biopsy. No mutations were identified in these genes. Whole exome sequencing analysis was performed in four members of this family and the same *FDX2* mutation detected in Family 1 was identified as the only segregating variant, homozygous in the two affected patients (Patients 5 and 6) and heterozygous in the parents of Patient 5.

The *FDX2* p.P144L variant affects a highly conserved residue that is identical in all mammals with an orthologous gene, and in invertebrates such as *Drosophila melanogaster* and *Caenorhabditis elegans*.

Functional validation of the *FDX2* mutation

Real-time RT-PCR was performed using muscle samples from Patients 3–6 and control muscle from two unrelated individuals. We identified no difference in *FDX2* mRNA expression between patients and controls (Fig. 4A).

To determine whether the mutation affected protein stability, we examined the FDX2 protein levels in muscle from Patients 3 and 6 (one patient from each family) and two unrelated controls by immunostaining. This revealed a severe reduction of FDX2 levels in patients as compared to controls. Equal protein loading was confirmed by Ponceau S staining (not shown) and by immunoblotting for a number of other mitochondrial (F1 α/β, VDAC) and cytosolic (actin, tubulin) proteins (Fig. 4B). The low amount of FDX2 in patient samples provides additional evidence that the *FDX2* p.P144L mutation is pathogenic.

Discussion

In this study, we describe a novel childhood onset disorder in two families with unusual clinical, radiological and

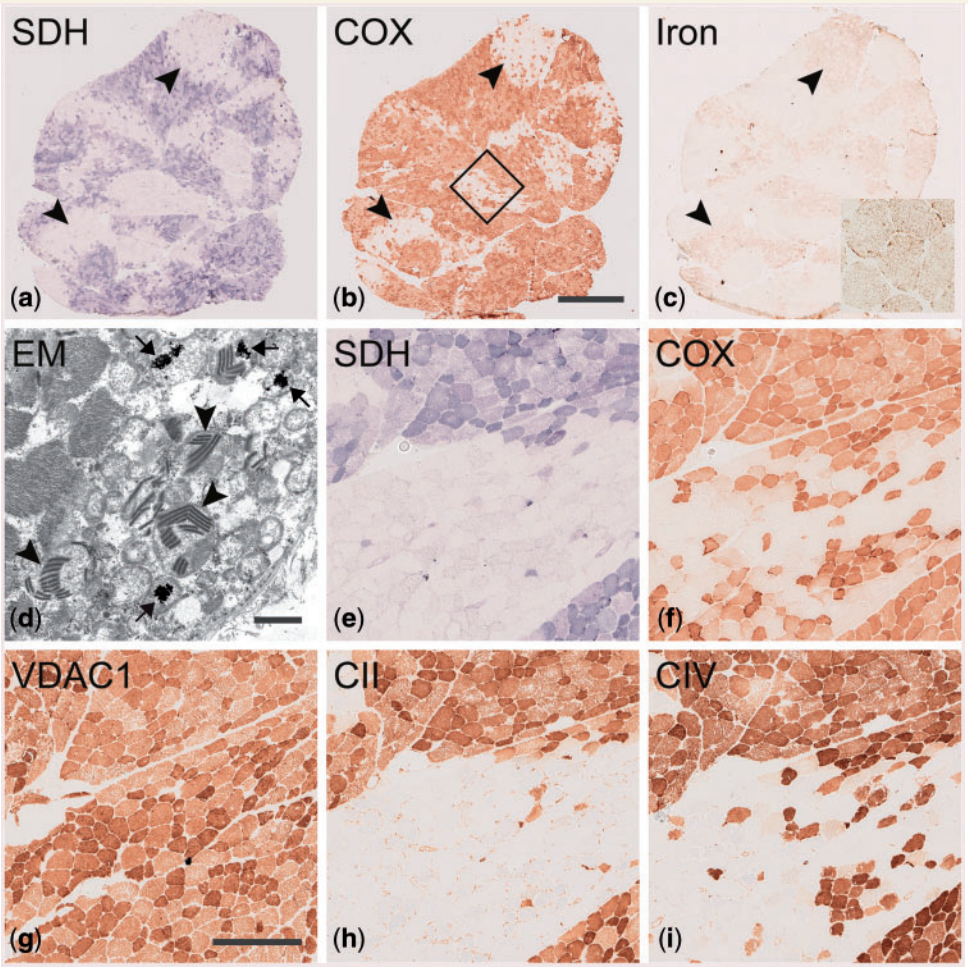

Figure 3 Muscle biopsy from Patient 3 demonstrating mitochondrial myopathy and iron deposition. (**A**–**C**) are serial sections showing an overview of the entire muscle biopsy cross-section. Note the focal deficiency of SDH and COX affecting numerous adjacent fibres in **A** and **B**, respectively and the associated deposition of iron in **C**. *Inset* in **C** shows fibres at higher magnification and punctate staining of iron. Electron microscopy in **D** shows electron dense inclusions presumably containing iron in mitochondria (arrows) and paracrystalline inclusions in mitochondria (arrowheads). (**E**–**I**) Serial sections demonstrating deficiency of complex II (**H**; subunit SDHB) and complex IV (**I**; subunit CO1) corresponding to the focal enzyme histochemical deficiency of SDH (**E**) and COX (**F**). Mitochondria are present in the corresponding regions as revealed by VDAC1 immunohistochemistry (**G**). The box in **B** marks the region shown at higher magnification in serial sections (**E**–**I**). Scale bar = 1 mm in **A**–**C** (bar shown in **B**). Scale bar in **D** = 1 μm. Scale bar = 250 μm in **E**–**I** (bar shown in **G**).

pathological features. The clinical syndrome included early-onset optic atrophy, recurrent episodes of myalgia with progressive myopathy, axonal polyneuropathy and a variety of haematological and endocrine abnormalities including microcytic anaemia, subclinical hypothyroidism, diabetes mellitus and reversible leukoencephalopathy. We used a combination of homozygosity and whole exome sequencing to identify the cause as a recurrent homozygous mutation in *FDX2*. We validated our findings genetically through segregation analysis and biochemically by demonstrating the almost complete absence of FDX2 protein by western blot in affected patient tissue.

Our clinical assessments of six patients with ages ranging from childhood to adult life allow us to infer the natural history of this disorder. Nystagmus and optic atrophy was the first sign of the disease and was present in the first 3 years of life in all six patients. Myopathic features developed during the first or second decade of life and presented with mild proximal weakness in limbs and/or recurrent acute episodes of myalgia and weakness precipitated by triggers such as cold weather and infections. Axonal neuropathy developed in the second decade or in adulthood leading to progressive distal weakness.

Interestingly, two individual reports have implicated mutations in *FDX2* causing a relatively discrete phenotype of mitochondrial myopathy and rhabdomyolysis without the additional features seen in our patients, or the unique radiological or pathological changes described here (Spiegel *et al.*, 2014; Lebigot *et al.*, 2017). Both previously reported cases shared the same mutation affecting the ATG start codon of *FDX2* (c.1A > T) and was predicted to lead to loss of *FDX2* expression. Despite normal mRNA levels of *FDX2*, we could demonstrate severely reduced protein expression in patient tissue, which could represent

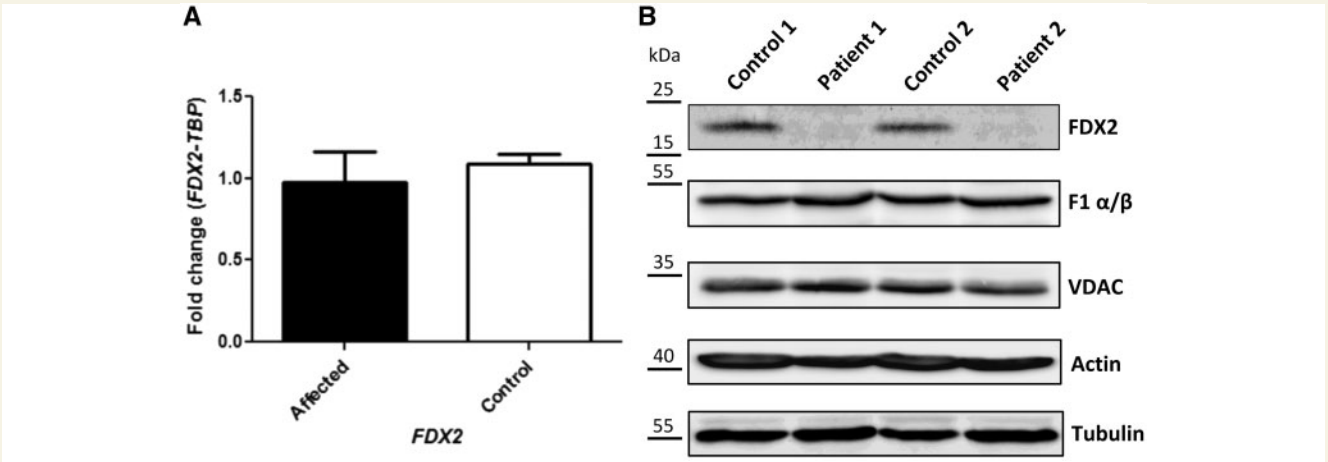

Figure 4 Functional studies. (**A**) RT-qPCR showing relative *FDX2* expression normalized to TBP in patients and controls. (**B**) Western blotting in patient and control muscle. Immunostaining was performed using specific antibodies against the mitochondrial protein FDX2, the F1 α/β subunits of complex V, and the voltage-dependent anion channel (VDAC, porin). Staining against actin and tubulin served as a loading control.

instability or excess degradation of misfolded or otherwise dysfunctional protein.

The extensive and multisystem involvement in our patients is reflected by the phenotype associated with mutations in the gene of an essential FDX2 interaction partner within the [Fe-S] cluster assembly machinery, *FDXR*, encoding ferredoxin reductase. These patients develop optic atrophy in addition to deafness and sensory neuropathy (Paul *et al.*, 2017).

Leukoencephalopathy is reported in several other disorders of [Fe-S] biogenesis, e.g. *NFU1* and *NUBPL* mutations. In *NUBPL* mutations (Kevelam *et al.*, 2013; Ahting *et al.*, 2015), some patients show progressive improvement of signal abnormality in the corpus callosum and cerebral white matter, although this occurs in the setting of clinical worsening over time (Kevelam *et al.*, 2013). In our patients we observed a progressive improvement of the white matter, thalamus and brainstem lesions compatible with reversible or partially reversible leukoencephalopathy. This finding is intriguing and further studies will be necessary to explain the improvement of the cerebral abnormalities. However defects in *MLC1*, *HEPACAM* and *CLCN2* cause leukoencephalopathies characterized by intramyelinic oedema (T-hyperintensity in subcortical white matter and corpus callosum, associated with restricted diffusion), and in some the intramyelinic oedema can be reversible (Depienne *et al.*, 2013). This may explain the reversibility seen in our patients in whom intramyelinic oedema was a feature.

Interestingly, we observed that the leukoencephalopathy did not show a clinical correlation. None of the three patients (Patients 1, 2 and 5) demonstrated any pyramidal or extrapyramidal signs at the time that the brain MRI demonstrated white matter, thalamus and brainstem abnormalities. Therefore, we can conclude the leukoencephalopathy related to the *FDX2* p.P144L mutation was reversible and asymptomatic in the patients here described. However, in two adult patients mild upper motor neuron signs were observed indicating that the pyramidal tracts may become involved over time. Follow-up of these patients can clarify this neurological finding.

The muscle histology in our patients is unusual, with a pattern characterized by fibres with mitochondrial proliferation in Gomori trichrome staining, and clusters of fibres that were SDH- and COX-negative. This histochemical abnormality is unusual for classical mitochondrial myopathies in which the ragged red fibres are SDH positive and COX negative (DiMauro and Gurgel-Giannetti, 2005). The histopathological findings are also different to findings in most cases of mitochondrial complex II deficiency, in which there are ragged red fibres that are SDH negative but positive in the COX reaction (Alston *et al.*, 2012). These findings are consistent with the function of FDX2 in the [Fe/S] cluster assembly of respiratory complexes I-III and heme A production for complex IV (Sheftel *et al.*, 2010). The immunohistochemical deficiency of subunits of complexes II and IV showed the same distribution as the enzyme histochemical deficiency of COX and SDH indicating that defective assembly of the respiratory chain complexes cause the enzyme deficiency. The patchy distribution of deficiency and variability from one cell to another remains unexplained.

The peculiar and characteristic regional SDH and COX deficiency and iron accumulation as revealed by iron staining and electron microscopy observed here have also been reported in ISCU myopathy (Olsson *et al.*, 2008; Kollberg *et al.*, 2009). These similarities suggest that both ISCU and FDX2 are important for cellular iron homeostasis via their role in the maturation of cytosolic IRP1 to an aconitase (Paul and Lill, 2015).

Defects in [Fe-S] cluster biogenesis are increasingly recognized as causing neurological disease. They play a critical role in mitochondrial function, which is exemplified by the varied neurological features in these cases, affecting the CNS as well as peripheral nerve and muscle. In conclusion, this study reveals that a biallelic mutation in *FDX2* causes

a complex childhood onset syndrome with unusual histopathological features, and confirms the important role that *FDX2* plays in mitochondrial health and disease.

Acknowledgements

Maurilio Pacheco e a Larissa Torres: logistic support in Alfenas (MG, Brazil).

Funding

This work was in part financed by Conselho Nacional de Desenvolvimento Científico e Tecnológico - CNPq, Fapemig, FAPESP-CEPID e INCT-CNPq; The Leonard Wolfson Experimental Neurology Centre, The Medical Research Council (MRC) and the Wellcome Trust. R.L. acknowledges generous financial support from Deutsche Forschungsgemeinschaft (SPP 1927) and networking support from the COST Action FeSBioNet (Contract CA15133). The Swedish Research Council Proj no 2012-02014 (to A.O.).

References

Ahting U, Mayr JA, Vanlander AV, Hardy SA, Santra S, Makowski C, et al. Clinical, biochemical, and genetic spectrum of seven patients with NFU1 deficiency. Front Genet 2015; 6: 123.

Alston CL, Davison JE, Meloni F, van der Westhuizen FH, He L, Hornig-Do HT, et al. Recessive germline SDHA and SDHB mutations causing leukodystrophy and isolated mitochondrial complex II deficiency. J Med Genet 2012; 49: 569–77.

Beilschmidt LK, Puccio HM. Mammalian Fe-S cluster biogenesis and its implication in disease. Biochimie 2014; 100: 48–60.

Beinert H, Holm RH, Münck E. Iron-sulfur clusters: nature's modular, multipurpose structures. Science 1997; 277: 653–9.

Boniecki MT, Freibert SA, Muhlenhoff U, Lill R, Cygler M. Structure and functional dynamics of the mitochondrial Fe/S cluster synthesis complex. Nat Commun 2017; 8: 1287.

Braymer JJ, Lill R. Iron-sulfur cluster biogenesis and trafficking in mitochondria. J Biol Chem 2017; 292: 12754–63.

Calvo SE, Tucker EJ, Compton AG, Kirby DM, Crawford G, Burtt NP, et al. High-throughput, pooled sequencing identifies mutations in NUBPL and FOXRED1 in human complex I deficiency. Nat Genet 2010; 42: 851–58.

Depienne C, Bugiani M, Dupuits C, Galanaud D, Touitou V, Postma N, et al. Brain white matter oedema due CIC-2 chloride chanel deficiency: an observational analytical study. Lancet Neurol 2013: 12: 659–68.

DiMauro S, Gurgel-Giannetti J. The expanding phenotype of mitochondrial myopathy. Curr Opin Neurol 2005; 18: 538–42.

DiMauro S, Servidei S, Zeviani M, DiRocco M, DeVivo DC, DiDonato S, et al. Cytochrome c oxidase deficiency in Leigh syndrome. Ann Neurol 1987; 22: 498–506.

Dürr A, Cossee M, Agid Y, Campuzano V, Mignard C, Penet C, et al. Clinical and genetic abnormalities in patients with Friedreich's ataxia. N Engl J Med 1996; 335: 1169–75.

Fontecave M. Iron-sulfur clusters: ever-expanding roles. Nat Chem Biol 2006; 2: 171–4.

Kevelam SH, Rodenburg RJ, Wolf NI, Ferreira P, Lunsing RJ, Nijtmans LG, et al. NUBPL mutations in patiens with complex I deficiency and distinct MRI pattern. Neurology 2013; 80: 1577–83.

Kollberg G, Tulinius M, Melberg A, Darin N, Andersen O, Holmgren D, et al. Clinical manifestation and a new ISCU mutation in iron–sulphur cluster deficiency myopathy. Brain 2009; 132(Pt 8): 2170–9.

Lebigot E, Gaignard P, Dorboz I, Slama A, Rio M, de Lonlay P, et al. Impact of mutations within the [Fe-S] cluster or the lipoic biosynthesis pathways on mitochondrial protein expression profiles in fibroblast from patients. Mol Genet Metab 2017; 122: 85–94.

Legati A, Reyes A, Ceccatelli Berti C, Stehling O, Marchet S, Lamperti C, et al. A novel de novo dominant mutation in ISCU associated with mitochondrial myopathy. J Med Genet 2017; 54: 815–24.

Lill R. Function and biogenesis of iron-sulphur proteins. Nature 2009; 460: 831–38.

Mochel F, Knight MA, Tong WH, Hernandez D, Ayyad K, Taivassalo T, et al. Splice mutation in iron-sulfur cluster scaffold protein ISCU causes myopathy with exercise intolerance. Am J Hum Genet 2008; 82: 652–60.

Naslavsky MS, Yamamoto GL, de Almeida TF, Ezquina SAM, Sunaga DY, Pho N, et al. Exomic variants of an elderly cohort of Brazilians in the ABraOM database. Hum Mutat 2017; 38: 751–63.

Nordin A, Larsson E, Thornell LE, Holmberg M. Tissue-specific splicing of ISCU results in a skeletal muscle phenotype in myopathy with lactic acidosis, while complete loss of ISCU results in early embryonic death in mice. Hum Genet 2011; 129: 371–78.

Olsson A, Lind L, Thornell LE, Holmberg M. Myopathy with lactic acidosis is linked to chromosome 12q23.3-24.11 and caused by an intron mutation in the ISCU gene resulting in a splicing defect. Hum Mol Genet 2008; 17: 1666–72.

Paul A, Drecourt A, Petit F, Deguine DD, Vasnier C, Oufadem M, et al. FDXR mutations cause sensorial neuropathies and expand the spectrum of mitocondrial Fe-S-Synthesis Diseases. Am J Hum Genet 2017; 101: 630–7.

Paul VD, Lill R. Biogenesis of cytosolic and nuclear iron-sulfur proteins and their role in genome stability. Biochim Biophys Acta 2015; 1853: 1528–39.

Purcell S, Neale B, Todd-Brown K, Thomas L, Ferreira MA, Bender D, et al. PLINK: a tool set for whole-genome association and population-based linkage analyses. Am J Hum Genet 2007; 81: 559–75.

Rouault TA. Iron-sulfur proteins hiding in plain sight. Nat Chem Biol 2015; 11: 442–5.

Schmittgen TD, Livak K. Analyzing real-time PCR data by the comparative C(T) method. Nat Protoc 2008; 3: 1101–08.

Sheftel AD, Stehling O, Pierik AJ, Netz DJ, Kerscher S, Elsässer HP, et al. Human ind1, an iron-sulfur cluster assembly factor for respiratory complex I. Mol Cell Biol 2009; 29: 6059–73.

Sheftel AD, Stehling O, Pierik AJ, Elsässer HP, Mühlenhoff U, Webert H, et al. Humans possess two mitochondrial ferredoxins, FDX1 and FDX2, with distinct roles in steroidogenesis, heme, and Fe/S cluster biosynthesis. Proc Natl Acad Sci USA 2010: 107: 11775–80.

Spiegel R, Saada A, Halvardson J, Soiferman D, Shaag A, Edvardson S, et al. Deleterious mutation in FDX1L gene is associated with a novel mitochondrial muscle myopathy. Eur J Hum Genet 2014; 22: 902–6.

Steeweg ME, Ghezzi D, Haack T, Abbink TE, Martinelli D, van Berkel CG, et al. Leukoencephalopathy with thalamus and brainstem involvement and high lactate 'LTBL'caused by EARS2 mutations. Brain 2012; 135(Pt 5): 1397–94.

Stehling O, Paul VD, Bergmann J, Basu S, Lill R. Biochemical analyses of human iron–sulfur protein biogenesis and of related diseases. Methods Enzymol 2018; 599: 227–63.

Stehling O, Wilbrecht C, Lill R. Mitochondrial iron–sulfur protein biogenesis and human disease. Biochimie 2014; 100: 61–77.

Stevens A. Pigments and minerals. In: Bancroft JD, Stevens A, editors. Theory and practice of histological techniques. Edinburgh: Churchill Livingstone; 1990. p. 245–67.

Webert H, Freibert SA, Gallo A, Heidenreich T, Linne U, Amlacher S, et al. Functional reconstitution of mitochondrial Fe/S cluster synthesis on Isu1 reveals the involvement of ferredoxin. Nat Commun 2014; 5: 5013.